Title
Analysis of Three Bridges That Exhibited Various Performance Levels in Liquefied and Laterally Spreading Ground

Journal
Journal of Geotechnical and Geoenvironmental Engineering, 139(7)

ISSN
1090-0241

Authors
Brandenberg, Scott J
Zhao, Minxing
Kashighandi, Pirooz

Publication Date
2013-07-01

DOI
10.1061/(asce)gt.1943-5606.0000832

Peer reviewed

June 17, 2013

Subject: "Analysis of Three Bridges That Exhibited Various Performance Levels in Liquefied and Laterally Spreading Ground," by Scott J. Brandenberg, Minxing Zhao, and Pirooz Kashighandi.
Author's draft version of paper published by the ASCE-GI Journal of Geotechnical and Geoenvironmental Engineering.

Interested Reader:

Due to the ASCE copyright transfer agreement, I am not permitted to openly distribute the final typeset version of the paper, but I am allowed to distribute the manuscript that I submitted to ASCE for final publication. This manuscript is not typeset, and is therefore not as convenient to read as the official version that can be downloaded at:

http://ascelibrary.org/doi/pdf/10.1061/%28ASCE%29GT.1943-5606.0000832

Sincerely,

Scott J. Brandenberg
Associate Professor
University of California, Los Angeles

Analysis of Three Bridges That Exhibited Various Performance Levels in Liquefied and Laterally Spreading Ground

by, Scott J. Brandenberg[1], M. ASCE., Minxing Zhao[2], and Pirooz Kashighandi[3]

Abstract: Three case histories of bridges supported on deep foundations that suffered various performance levels in liquefied and laterally spreading ground are analyzed using a beam on nonlinear Winkler foundation method. The exhibited performance levels were no measurable foundation deformation, moderate damage, and collapse. Analyses are first performed using the best available information regarding ground motions and free-field lateral spreading surface displacements. Predictions closely match observations when the inputs are well known. The cases are subsequently re-analyzed using a probabilistic forward prediction that incorporates uncertainty in the ground motion prediction, liquefaction triggering evaluation, lateral spreading surface displacement, and structural response. Significant differences in lateral spreading displacements estimating by different methods introduced significant dispersion into predictions of structural response for cases of poor performance in which the piles moved with the spreading soil, but had little influence for cases with good performance where the liquefied soil spread around a

[1] Associate Professor, Department of Civil and Environmental Engineering, University of California, Los Angeles, 90095, email: sjbrandenberg@ucla.edu; Corresponding Author

[2] Project Engineer, CH2M Hill, 6 Hutton Centre Drive Santa Ana, CA 92707, email zhaomx06@gmail.com

[3] Project Engineer, Diaz Yourman Associates, 1616 East 17th Street, Santa Ana, CA 92705-8509, email pirooz@diazyourman.com

stiff pile foundation.

Introduction

Liquefaction and lateral spreading has affected many bridges in past earthquakes inducing damage that ranged from negligible, to moderate, to collapse. Examples of collapse include the Showa Bridge (Hamada and O'Rourke 1992) and Nishinomiya Bridge (Wilson 2003), where excessive deformation of the piers caused unseating of simply-supported spans. The Landing Road Bridge suffered moderate, reparable damage as a result of as much as 2m of lateral spreading of a nonliquefiable crust layer over liquefied sand (Berrill et al. 2001). The Leuw-Mei Bridge is an example of good performance of the bridge foundation despite nearby lateral spreading caused by the 1999 Chi-Chi earthquake. Lateral spreading of as much as 0.25m near the bridge was documented by Chu et al. (2006), but liquefaction-induced damage was not evident although the bridge did suffer damage to its bearings due to strong shaking (Chu et al. 2008).

Recent experimental modeling studies have clarified fundamental aspects of interaction of deep foundations in liquefied and laterally spreading ground (e.g., Boulanger and Tokimatsu 2006), and led to development of multiple analysis methods. However, only a handful of studies have applied these analysis methods to case histories, and the focus tends to be on poor performance in the few cases where case histories are analyzed. . For example, Dobry et al. (2003) analyzed the Niigata Family Courthouse Building, whose piles suffered extensive damage, Berrill et al. (2001) and Ledezma and

Bray (2010) analyzed Landing Road Bridge that suffered moderate damage, and Kerciku et al. (2008) studied the collapse of Showa Bridge postulating a buckling instability in the piles as the cause of collapse. These studies focused on cases where bridges were damaged by lateral spreading, and very little attention has been given to bridges that performed well despite liquefaction and lateral spreading. Predicting good performance is obviously important. Furthermore, previous case history back-analyses have taken great care to utilize measured inputs wherever possible (e.g., free-field lateral spreading surface displacement), hence the predictive accuracy is conditioned on very good understanding of the input parameters. On the other hand, forward predictions do not have the luxury of measured inputs, and uncertainty must be considered. Little effort has focused on quantifying the various sources of uncertainty that contribute to liquefaction hazard for bridges, including ground motion, liquefaction triggering, lateral spreading displacements, and structural response.

This paper presents analysis of the Showa, Landing Road, and Leuw-Mei Bridges (Figs. 1, 2, and 3) that experienced collapse, moderate damage, and no measurable liquefaction-induced damage, respectively. The case histories are first analyzed deterministically using a beam on nonlinear Winkler foundation (BNWF) method combined with measured values for input parameters such as nearest measured peak ground acceleration and free-field lateral spreading ground surface displacement. This set of analyses demonstrates how well the BNWF predictions agree with the measured response of each bridge when the inputs are accurately characterized. The case histories are then re-analyzed by assuming that the free-field lateral spreading ground displacement and inertia demands are unknown and must be estimated from the earthquake scenario and site conditions. Results are presented as probability of exceedance of various relevant engineering demand parameters (e.g., pile cap rotation, pier column rotation) conditioned on the earthquake scenario and site conditions.

Case History Descriptions

Showa Bridge

The Showa Bridge had recently been constructed across the Shinano River in Niigata City when the M_w 7.5 1964 Niigata earthquake liquefied the surrounding soil causing collapse of five spans (Fukuoka 1966). The bridge is approximately 40km from the epicenter of the earthquake, and 1.2km from the nearest strong motion recording in the basement of a building at Kawagishi Cho, where the peak horizontal acceleration was 0.16g (Table 1) and peak transient displacements were near 0.4m. The bridge has a width of 24m and total length of 304m divided among 12 simply-supported steel I-girder spans (Fig. 1). The ends of the I-girders were supported by 1.3m wide bent caps. Some spans were connected to the bent cap by pin connections (denoted F in Fig. 1), while other spans rested directly atop the bent cap (M in Fig. 1). Each bent cap was supported by a row of nine 0.61m diameter 25m long steel pipes that formed the piles and the pier columns, and each pile supported an axial load of 740kN (Bhattacharya et al. 2003). The pipes were tied together by the bent cap and by a pile cap near the water line. The wall thickness of the pipes was 16mm in the upper 12m, and 9mm in the lower 13m. The yield bending moment and yield curvature in the upper region are 2153kN·m and $0.0078m^{-1}$, respectively, and in the lower region are 1254kN·m and $0.0078m^{-1}$, respectively.

The Showa Bridge collapsed as a result of liquefaction of loose alluvium that was approximately 10m thick on the left side and thinner on the right side of the river. The extent of the liquefiable soils shown in Fig. 4 was based on blow counts presented by Hamada and O'Rourke (1992). Five spans unseated between piers P_2 and P_7, where the liquefiable soils are thickest. The unseating failures occurred at the M connections, with the exception of the span between piers P_5 and P_6, where an F connection also failed and the span collapsed completely into the river. The left bank of the Showa Bridge exhibited lateral spreading of as much as 3m toward the river (Hamada and O'Rourke 1992), and the right bank spread by about 0.5m toward the river.

Reliable eyewitness accounts indicate that the unseating failures occurred after shaking had subsided, and therefore the failures could not have been caused by inertia demands (Yoshida et al. 2007). Furthermore, liquefaction flow failure of the left revetment occurred after the bridge was observed to have collapsed, which led Yoshida et al. to conclude that flow liquefaction was not a probable cause of the bridge failure. Delayed ground deformations can be caused by void redistribution during post-liquefaction reconsolidation (e.g., Kulasingam et al. 2004). Possible explanations for the bridge failure are transient ground deformations induced by strong shaking, permanent ground deformations caused by lateral spreading that were smaller than the final flow deformations observed at the left revetment, buckling instability (e.g., Bhattacharya et al. 2003) or a combined flexure-buckling mechanism of the piles in the liquefied sand.

Landing Road Bridge

The Landing Road Bridge was constructed in 1962 and was moderately damaged by liquefaction and lateral spreading due to the M_w 6.3 1987 Edgecumbe earthquake. The bridge is approximately 8km from the nearest fault rupture, and approximately 22km from the nearest strong motion record at the Matahina Dam (also about 8km from the nearest fault rupture) where the peak ground acceleration was 0.29g. The bridge consists of 13 spans, each 18.3m long, constructed of five precast post-tensioned concrete I-beams bearing on 16mm thick rubber pads. The spans are bolted together, to the abutments, and to the piers, thereby forming an essentially continuous superstructure and stiff moment-resisting connections to the piers and abutments. The substructure comprises concrete pier walls running the full width of the superstructure, each supported by eight 0.41m square prestressed concrete piles at a 6:1 batter. The piles were fixed into pile caps embedded about 0.5m below the ground surface, and pile cap dimensions were approximately 10m long (in the transverse bridge direction) 2m wide and 0.75m tall.

The liquefiable geologic feature was the flood plain on the left bank of the Whakatane River in which five of the bridge piers and the left abutment were founded. The right bank was composed of stiffer sediments that were not susceptible to liquefaction. The left bank deposit consisted of a nonliquefiable silty crust approximately 1.2m thick over loose liquefiable sand with average fines content of about 12%, over dense sandy material. The crust spread laterally by as much as 2m at the river bank and displacements extended 300m back from the river bank. Spreading is believed to have occurred in a static mode after strong shaking based on eye witness accounts that the road was passable immediately after the earthquake, but not an hour later. The 1.2m thick nonliquefiable crust was composed of silty materials with mixed in wood chips that had been deposited on the banks of the river by a nearby cardboard mill. Berrill et al. (2001) suggested that $\phi=25°$ and c=10kPa are appropriate strength parameters based on their detailed site investigation, and the unit weight is only 12.5kN/m^3 due to the presence of wood chips.

The bridge suffered damage to its pier walls and left abutment, and the superstructure did not sustain any significant damage, though buckled footpaths indicated compressive forces were mobilized in the superstructure. Some of the piers suffered rotations of about 1° and cracks that were repaired with epoxy resin. Small cracks were also observed near the heads of some of the piles. Ground settlements of 0.3 to 0.5m were observed at the approach to the left abutment. Structural analyses by Berrill et al. (2001) predicted that collapse loads were nearly mobilized against the bridge.

Leuw Mei Bridge

The Leuw-Mei Bridge was strongly shaken by the M_w 7.6 1999 Chi-Chi earthquake, and suffered damage to its bearings due to strong shaking, but exhibited no discernible permanent foundation deformations despite liquefaction and lateral spreading of nearby soil deposits. The bridge is approximately 0.6km from the nearest fault rupture, and approximately 0.5km from the nearest strong motion recording at the TCU076 station, where the peak horizontal acceleration of 0.42g was measured in the fault parallel direction. The 7-span curved Leuw Mei Bridge was constructed over the Miao-Lo River in 1998 as a replacement of a previous bridge (Chu et al. 2008). The bridge is 10.1m wide and the superstructure consists of six reinforced concrete box girders ranging in length from 21m to 28m, and one 140m-long steel cable-stay center span. The girders are simply supported on reinforced concrete bearings at the top of the 2.5m diameter reinforced concrete pier columns. The pier columns are founded on large 5m diameter reinforced concrete caissons embedded to a depth of 17m.

Lateral spreading was documented along the bank about 100m north of the bridge by Chu et al. (2006) at a site referred to as "Nantou Site N" (borings NCS-1 and NCS-2 in Fig. 4). A saturated silty sand deposit with high content of non-plastic fines (SP to ML) was determined to have liquefied and caused the observed lateral spreading deformations of as much as 0.25m toward the Miao-Lo River. The water table was at a depth of one meter at the time of their investigation. Lateral spreading was observed on both river banks both upstream and downstream of the river, but documentation by Chu et al. (2006) focused only on one bank to the north of the bridge.

Beam on Nonlinear Winkler Foundation Analyses

Static beam on nonlinear Winkler foundation (BNWF) numerical simulations were performed using the finite element modeling platform OpenSees (McKenna 1997). Piers and piles were modeled using nonlinear beam column elements with the post-yield flexural stiffness equal to 5% of the elastic stiffness. Pile caps were modeled using stiff (essentially rigid) elastic beam column elements, and soil-structure interaction elements (p-y for lateral, t-z for friction and q-z for end bearing) were attached to embedded portions of the structure. Lateral spreading demands were imposed as displacements on the free-ends of the p-y elements. Inertia demands compatible with the effects of liquefaction were included for Leuw Mei Bridge, but not for Showa Bridge and Landing Road Bridge since lateral ground deformations and bridge damage occurred after strong shaking had ceased. Inertia demands at Leuw Mei Bridge were represented as forces applied at the top of the pier column, and were estimated using the procedure documented by Boulanger et al. (2007) in which the peak horizontal surface acceleration is multiplied by reduction factors that account for the influence of liquefaction on ground motion and phasing between kinematic and inertia demands. The demands were increased linearly using small enough increments to facilitate numerical convergence. The convergence test was based on the norm of the displacement increments (i.e., the NormDispIncr test in OpenSees), and the tolerance was set to 10^{-6}. Penalty constraints were utilized to enforce prescribed displacement boundary conditions. Newton Raphson iteration was used to solve the nonlinear systems of equations. A P-Δ transformation was utilized.

Properties of the p-y elements were first defined based on the API (2003) relation for nonliquefied sand and subsequently multiplied by a p-multiplier, m_p to account for the effects of liquefaction. The nonliquefied p-y properties required input of friction angle and subgrade reaction modulus. The peak friction angle was estimated using concepts from critical state soil mechanics by (1) computing relative density as $D_R = \sqrt{\frac{(N_1)_{60}}{46}}$ following Idriss and Boulanger (2007), (2) estimating the critical state friction angle as ϕ'_{cs}=32° for quartz sand (Bolton 1986), and (3) computing the difference between peak and critical state friction angle as $\phi'_{pk} - \phi'_{cs} = 3[D_R(10\text{-ln } p')\text{-}1]$ following Bolton (1986). Subgrade reaction values were estimated based on Terzaghi (1955).

The m_p values recommended by Brandenberg (2005) were used for fully liquefied sand (i.e., $FS_{liq} \leq 1.0$). For cases with $FS_{liq} > 1.0$, the excess pore pressure ratio, r_u, was estimated following Marcuson and Hynes (1990), and the m_p value was linearly interpolated between its fully-liquefied value and its fully nonliquefied value following Dobry et al. (1995). . The p-multiplier approach fails to capture many fundamental features of p-y response in liquefiable soil such as dilatancy, permeability, and rate effects that have been observed in past physical model studies and numerical simulations [e.g., Wilson et al. (2000), Rollins et al. (2005), González et al. (2009)]. Nevertheless, the maximum bending moments and pile head displacements computed using this method have shown reasonable agreement with measurements in past studies (e.g., Ashford and Juirnarongrit, 2003; Brandenberg et al. 2007) and the method is widely utilized to analyze the effects of lateral spreading on pile foundations. Table 2 summarizes the input parameters used to generate the soil-structure interaction elements for each component analyzed herein.

Deterministic Analyses Using Measured Ground Displacements as Inputs

To assess the predictive ability of the BWNF method using a common set of inputs, measured lateral spreading ground displacements were used to guide the selection of a free-field displacement profile that was imposed on the free-ends of the p-y elements. The ground surface displacement was measured at each site, but the profile of subsurface displacement was not measured and assumptions had to be made. For simplicity, shear strain in the liquefiable loose sand layer was assumed constant, and some small shear strain was imposed in the underlying nonliquefied dense layers based on the factor of safety against liquefaction using the relationship by Zhang et al. (2004). Shear strain in any over-riding nonliquefied crust layer was assumed zero. Additionally, slip at the interface between a nonliquefied crust and underlying liquefiable layers was applied for Landing Road Bridge, where a permeability contrast was anticipated. Such displacement discontinuities are caused by void redistribution and have been observed in a number of modeling studies (e.g., Kulasingam et al. 2004). An accurate quantitative method for predicting the amount of interface slip caused by void redistribution does not currently exist, though past studies provide qualitative evidence that slip likely caused much of the surface displacement. The slip was assumed to constitute half of the measured surface displacement, with the other half arising from shear strain in the liquefied sand. Assumptions regarding interface slip are anticipated to have a small effect on pile response due to the dominant presence of the nonliquefied crust in typical lateral spreading problems (e.g., Dobry et al. 2003).

Boulanger et al. (2007) used numerical simulations calibrated with centrifuge model tests to characterize liquefaction-compatible inertia demands using two factors; C_{liq} that characterizes the peak inertia demand with liquefaction divided by that without liquefaction, and C_{cc} that characterizes phasing of kinematic and inertia demands defined as inertia demand at the time that the peak bending moment occurred in the piles divided by the peak inertia demand. Inertia forces were omitted for Showa Bridge and Landing Road Bridge since these bridges were observed to fail in the static mode after strong shaking. Inertia forces imposed on the Leuw-Mei Bridge were computed as tributary superstructure mass multiplied by the peak ground surface acceleration multiplied by C_{liq} = 0.6 and C_{cc} = 0.6 as suggested by Boulanger et al. (2007) for motions with typical spectral shape.

Showa Bridge

Fig. 5 shows the displacement, bending moment, and subgrade reaction profiles for pier P_4 for the Showa Bridge. A final surface displacement of 3m was specified in the finite element analysis to be consistent with field measurements. However, convergence failure occurred when the ground surface displacement reached about 0.9m as a result of a collapse mechanism caused by the large pier top displacement combined with the P-Δ transformation. Fig. 5 shows the last converged time step, beyond which the analysis became unstable. The displacement of the top of the pier column was about 2.4m when the ground surface displacement reached 0.9m. An unseating failure would be anticipated prior to formation of the collapse mechanism since the seat length is only about 0.6m. The measured pile head deformation for piles extracted after the earthquake was about

1m, which is less than predicted although continued displacement may have arrested following collapse due to removal of the P-Δ moment. The conclusion is that the analysis accurately predicts that a collapse mechanism occurred at P_4 for the Showa Bridge.

Fig. 6 shows the displacement, bending moment, and subgrade reaction profiles for pier P_9 on the right side of Showa Bridge where the liquefiable deposit was thinner, lateral spreading surface displacements were smaller (about 0.5m compared with 3m), and spans did not collapse into the river. A ground surface displacement of 0.5m was imposed on P_9, and the displacement at the top of the pier column reached about 0.12m. Unlike the analysis of P_4, a collapse mechanism did not form during analysis of P_9 and the predicted pier top displacement is less than the seat length of 0.6m. Hence non-collapse of the span is accurately predicted. The difference between P_4 and P_9 is that the loose sand was considerably thicker at P_4, and embedment into the dense nonliquefied sand was much less. As a result, P_4 essentially moved with the soil, whereas P_9 exhibited adequate embedment to allow the liquefiable sand to flow around it during lateral spreading.

Landing Road Bridge

Fig. 7 shows the displacement, bending moment, and subgrade reaction profiles for a pier at the Landing Road Bridge. The top of the pier column was fixed against displacement and rotation, which is consistent with the observations that (1) the pier columns were bolted to the superstructure, forming stiff moment-resisting connections, and (2) components on the other side of the river were founded in nonliquefiable soils, and components positioned in the river had been retrofitted by installation of large-diameter deep foundations.. The post-earthquake observation of superstructure displacement being smaller than pile cap displacements in the lateral spread indicates that the retrofitted components in the river and in nonliquefiable ground on the other side of the river were adequately strong to essentially hold the superstructure fixed despite lateral spreading demands. A free-field soil displacement pattern with 2m amplitude at the surface was imposed, and the soil deformation profile exhibited a discontinuity at the interface between the silt and underlying liquefied sand. The pile cap displacement was about 0.1m, which corresponds to a pier column rotation of about 1°. The top and bottom of the pier column exhibited bending moments that are higher than the yield bending moment of 692kN·m estimated by Berrill et al. (2001). The reported bending moment for the piles is the combined value for all four out-of-plane piles in the group. The mobilized bending moments are larger than the yield moment of 931kN·m. The observation of some yielding of the pier column and piles is consistent with the observation that cracking occurred in the piles and pier columns, and was subsequently repaired by epoxy grouting (Berrill et al. 2001), and the predicted pier column rotation of about 1° is consistent with the measured rotation.

Leuw Mei Bridge

Fig. 8 shows the displacement, bending moment, and subgrade reaction profiles for the caisson and pier column at the Leuw-Mei Bridge. In this case the measured free-field lateral spreading surface displacement was 0.25m. An inertia load of 808 kN was imposed at the top of the pier column, and was computed using C_{liq} = 0.6 and C_{cc} = 0.6, following the recommendation of Boulanger et al. (2007) for ground motions with medium frequency content (F_I=0.6*0.6*0.42g*9.81m/s^2*545Mg=808kN). The resulting displacement predicted at the top of the pier column was about 0.03m, which is due nearly entirely to the flexural deformation of the pier column under the imposed inertia demand. Negligible displacement and rotation of the caisson is predicted in the analysis. This prediction is consistent with the observations following the earthquake that negligible foundation deformation occurred.

Probabilistic Analysis

The three preceding analyses indicate that the BNWF method can accurately predict the response of pile foundations in liquefied ground provided that input parameters such as ground motions and free-field lateral spreading ground displacements are well known. However, many inputs are highly uncertain and cannot be reasonably known for a forward analysis. Uncertain inputs include the ground motion, liquefaction triggering, free-field lateral spreading ground surface displacement, liquefaction-compatible inertia demand, properties of the p-y elements, and strength and stiffness of the structural elements. The remaining sections of this paper explore how uncertainty in estimating the input parameters affects the prediction of structural damage caused by liquefaction and lateral spreading.

Ground Motion Prediction

The mean and standard deviation of the peak horizontal ground accelerations were estimated using the NGA ground motion prediction equations (Abrahamson et al. 2008) using OpenSHA (Field et al. 2003) for the Edgecumbe and Chi-Chi earthquakes, and Zhao et al. (2006) for the Niigata earthquake. The NGA models are appropriate for the Edgecumbe and Chi-Chi earthquakes, since these were shallow crustal events (in fact ground motions from both earthquakes appear in the NGA database). However, the NGA models are not appropriate for the deeper Niigata interface earthquake, so the Japan-specific Zhao et al. (2006) model was used instead. Estimates are summarized in Table 3. In addition to the style of faulting, moment magnitude, and V_{s30}, many other input parameters are required for the NGA relations. All three earthquakes ruptured the surface, so the depth to fault rupture, Z_{TOR}, is zero in each case. Only Landing Road Bridge was on the hanging wall of the fault; the other two sites were on the footwall. The depth to stiff soil (i.e., either $Z_{1.0}$ or $Z_{2.5}$) is not known at any site, and an average value of 0.5 km was input to the models. However, this parameter has very little or zero influence on PGA, which is used for liquefaction triggering. The GMPE by Idriss (2008) was not utilized in this study because V_{s30} for all three sites is less than the range from 450 to 900 m/s Idriss considered in development of his GMPE. None of the borings extended to a depth of 30 m. To estimate V_{s30}, the lowest $(N_1)_{60}$ value was assumed to extend to 30m. This assumption had little influence on the computed V_{s30} value because the layers beneath the bottom of the boring logs tended to be stiff, whereas the calculation of V_{s30} weights soft layers more heavily than stiff layers. .

The Kawagishi Cho recording station and Showa Bridge both classify as Site Class D based on V_{s30}, and Site Class F based on occurrence of liquefaction. On the other hand, the recording stations nearest to the Landing Road and Leuw Mei bridges classified as Site Class C, whereas the Landing Road Bridge and Leuw Mei bridge sites classify as Site Class D based on V_{s30}, and Site Class F when liquefaction potential is considered. The nearest recorded motions are presented herein without adjustment for differences in site class due to uncertainty in the amplification factors. Ledezma and Bray (2010) found the difference in site class had a small influence on median predicted ground motions at Landing Road Bridge, and did not adjust for site class.

Liquefaction Triggering Evaluation

Liquefaction triggering evaluation was performed using methods by Idriss and Boulanger (2006) and by Cetin et al. (2004). Energy corrections were based on energy measurements for Leuw Mei Bridge (Chu et al. 2006) and based on hammer type for the other two bridges. Corrections for rod length, borehole diameter, and sampler liner were based on the suggestions by Youd et al. (2001). Average fines content was specified as 12% by Berrill et al. (2001) for the Landing Road Bridge, and fines content was estimated to be 10% for the Showa Bridge based on measurements from similar soils at a nearby bridge (Hamada and O'Rourke 1992). The fines contents associated with each blow count were reported by Chu et al. (2006) for Leuw Mei Bridge. Overburden correction C_N, fines correction, MSF, K_σ, and r_d values were computed in accordance with each triggering procedure.

Fig. 4 shows cyclic stress ratio, CSR, versus corrected SPT blow count, $(N_1)_{60cs}$, for the available SPT data. CSR was computed using the nearest measured PGA reported in Table 3, and these values are shown as symbols in Fig. 4. The error bars in Fig. 4 correspond to the median GMPE prediction ±1σ. Data points in Fig. 4 are plotted with open symbols if they plot to the right of the triggering curves (indicating liquefaction will not trigger), closed symbols if they plot to the left of the curves, and open/closed if they plot between the two curves. Blow counts for clay are plotted in open stars and for gravel as open plus signs at Leuw Mei Bridge, and all other blow counts are for materials that are potentially susceptible to liquefaction. The gravel deposit at Leuw Mei Bridge may be susceptible to liquefaction due to the lower-permeability sand layer resting atop the gravel. Hence, the gravel is treated as liquefiable in one set of analyses and nonliquefiable in another set to observe the influence. Corrections to blow counts for fines and overburden, and corrections to CSR for overburden and magnitude were based on Idriss and Boulanger (2006). Slight differences in $(N_1)_{60cs}$ and CSR would arise using Cetin et al. (2004), but the differences have essentially no influence on conclusions drawn from the triggering evaluation.

Regardless of which liquefaction triggering curve is utilized, or whether the nearest measured or mean predicted ground motions are utilized, some of the blow counts at each site indicate the presence of liquefiable sands, which is consistent with case history observations that these sites liquefied.

Lateral Spreading Displacement Predictions

Given that liquefaction triggering is expected at each site, the next step involves estimating the free-field lateral spreading ground displacement, D_H. Multiple methods exist for estimating lateral spreading ground displacements, and can give significantly different predictions. This epistemic uncertainty is important and should not be neglected, so cumulative distribution functions of lateral spreading displacement conditioned on the earthquake scenario and soil conditions were computed for each site using three different methods: the empirical multiple linear regression equation presented by Youd et al. (2002), the liquefaction displacement index model presented by Faris et al. (2006), and a Newmark sliding block procedure that is similar to that presented by Olson and Johnson (2008).

For the Youd et al. (2002) procedure the sloping ground equation was adopted (as opposed to the free-face equation) since none of the piers analyzed in this study were behind a free face. Slope angles were measured and reported in the literature at Leuw Mei and Landing Road Bridges, and the slope of the river bottom at Showa Bridge was taken to be 1%. Table 4 presents the ground displacement estimates. The Youd et al. (2002) method is formulated deterministically, though the database of ground displacements utilized to construct the regression equation is publicly available for estimating the distribution of the measurement error. Prediction errors were computed as the natural log of the predicted value minus the natural log of the measured value, and the standard deviation of the prediction errors was computed as 0.45. Hence, D_H was assumed to be log-normally distributed with the median value computed from the sloping ground equation and the natural log standard deviation of D_H equal to 0.45, and distributions are shown in Fig. 9.

The displacement potential index (DPI) method presented by Faris et al. (2006) relates free-field lateral spreading ground displacement to the strain potential index, SPI, based on the maximum single-amplitude shear strain mobilized during cyclic simple shear tests published by Wu (2002). The equations for average displacement using the simplified model from Faris et al. is used herein. An example calculation of D_H using the DPI method is shown in Table 5 for boring NCS-2 at Leuw Mei Bridge. Faris et al. selected case histories in which the ground motion was measured near the lateral spread feature such that the distribution of D_H is conditioned on accurate knowledge of the ground motion. Hence, ground motion uncertainty is not implicit in the method and must be included separately. Monte Carlo simulation was used to define the distribution of D_H by repeating the calculation 100,000 times and observing the distribution of D_H (Fig. 9).

The Newmark sliding block procedure was studied by Olson and Johnson (2008) to analyze case histories of lateral spreads utilizing liquefied undrained residual strength, s_r, and they found that the back-calculated strengths were consistent with those from flow slide case histories (Olson and Stark 2002). Their method is utilized herein with the average trend line for s_r/σ_{vc}'. Furthermore, Newmark displacements were estimated using the procedure by Bray and Travasarou (2007) rather than the method by Jibson and Jibson (2003) that was utilized by Olson and Johnson.

Selecting a representative blow count for estimating s_r depends on the particular site and the lateral continuity of the liquefiable layer relative to the anticipated slide mass. In this case, the $(N_1)_{60}$ values with $FS_{liq}<1.0$ in the vicinity of the foundation being analyzed were averaged because a horizontally continuous sub-layer within the liquefiable zone was not identified. The yield acceleration was computed using an infinite slope procedure because the geometry of the slope near the foundations could be reasonably approximated by an infinite slope.

The Bray and Travasarou (2007) method for computing slope displacements assumes perfect knowledge of the yield acceleration of the slope, k_y, since this was directly specified as an input parameter in the stick-slip model used to derive the equations. However, uncertainty in the liquefied undrained residual strength renders k_y uncertain, and this uncertainty should be included explicitly in the analysis. Olson and Stark (2002) specified that the standard deviation of the undrained residual strength ratio was 0.025. Low undrained residual strengths can result in a flow slide condition (i.e., $k_y<0$), in which the Bray and Travasarou method should not be used and large displacements should be anticipated. An example calculation demonstrating the method is shown in Table 7 using the median values of the input parameters. The Monte Carlo method with 100,000 realizations was utilized to compute the cumulative distribution function of D_H (Fig. 9).

The three methods exhibit significant variation in the distributions of D_H. No single method was uniformly the most accurate for every case history. Faris et al. was more accurate for the Showa Bridge and Landing Road Bridge, both of which exhibited post-shaking lateral spreading deformations, and the Newmark method significantly underpredicted displacements at these sites. The Newmark method produced the most accurate result for the Leuw Mei Bridge, where occurrence of post-shaking lateral spreading is unclear. A possibility is that the Leuw Mei lateral spread was inertia driven, and therefore well-suited for a Newmark-type analysis.

Differences in the predictions are caused by differences in the assumptions inherent in the models. For example, the Youd et al. method assumes that all blow counts less than 15 contribute equally to lateral spreading, whereas blow counts over 15 do not contribute at all. The other two methods distinguish the effects of blow count on a more continuous scale. The Newmark sliding block method is quite sensitive to ground motion, whereas the Youd et al. method and the Faris et al. method are not as sensitive because the Youd et al. method uses M_w and R as input variables (rather than PGA), and the SPI values used in the Faris et al. model reach a limit at high CSR and therefore become insensitive to ground motion. Furthermore, thickness of the liquefiable layer is important in the Faris et al. and Youd et al. methods, and relatively unimportant for the Newmark method.

Treating the gravel layer as liquefiable at Leuw Mei Bridge influenced only the Faris prediction because (i) the increase in T_{15} in the Youd et al. method increases the already large lateral spreading displacements to even larger numbers that have little physical significance, and (ii) the gravel had no influence on selecting the representative blow count for the horizontally continuous sliding plane for the Newmark analysis.

Structural Response

Sources of uncertainty in the structural response analysis include the properties of the p-y materials, the distribution of free-field lateral spreading displacement with depth, the liquefaction-compatible inertia demand, and the capacity and stiffness of the structural components. These sources of uncertainty were quantified as the probability of exceedance of a relevant engineering demand parameter, EDP, as a function of free-field lateral spreading surface displacement [i.e., $P(EDP>edp \mid D_H = d_h)$], herein called fragility functions. The most important EDP's for each bridge were determined to be the displacement of the top of the pier column for Showa Bridge, the displacement of the top of the caisson for Leuw Mei Bridge, and the pier column rotation for the Landing Road Bridge. These EDP's were selected to facilitate comparison with the measured response of each bridge (i.e., unseating collapse for Showa Bridge, lack of measurable foundation displacement at Leuw Mei Bridge, and ~1° pier column rotation at Landing Road Bridge. Distributions were assigned to the input parameters, as summarized in Table 8. The standard deviation for the p-multipliers (m_p) applied to the p-y materials on the piles was selected to cover the range of values suggested by various researchers, as summarized by Brandenberg (2005). The amount of slip at the interface between a nonliquefied low-permeability crust and the underlying liquefied sand was controlled by a uniformly-distributed random variable quantifying the ratio of slip at the interface to the ground surface displacement. Liquefaction-compatible inertia demands were imposed following suggestions of Boulanger et al. (2007), and the standard deviations of C_{liq} and C_{cc} were approximately 0.7. The inertia demands were imposed on the top of the pier column simultaneously with applied free-field lateral spreading displacement profile. The Monte Carlo method with 1000 realizations was utilized to define the fragility functions (i.e., 1000 BNWF analyses were performed in OpenSees for each case, and the inputs were randomly selected from their distributions).

The fragility functions are presented in Fig. 10 for the three bridges. For Showa Bridge P_4, on the left side of where liquefied deposits were thick, the piles essentially move with the spreading soil and the pier top displacement is therefore very sensitive to ground deformation. Hence, the fragility functions are nearly vertical. For Showa Bridge P_9, on the right side where liquefiable deposits are thinner, the pier column is less sensitive to free-field ground surface displacement, and the influence of other uncertain variables renders more dispersion in the fragility function. The predicted displacements of the caisson at the ground level at Leuw Mei Bridge are on the order of a few millimeters when the gravel layer is treated as non-susceptible to liquefaction, and on the order of a few centimeters when the gravel layer is treated as susceptible. These findings are consistent with the lack of observation of foundation deformation due to lateral spreading at this site. . Furthermore, the fragility functions are very flat, which indicates that free-field surface displacement exerts small influence on the caisson deformations compared with other uncertain variables such as inertia demands. For Landing Road Bridge the median predicted pier column rotation conditioned on the measured free-field lateral spreading ground displacement of 2m is about 3% (1.8°). This is reasonably consistent with the measured rotation of 2% (1°) of permanent pier rotation.

Probability of Exceedance of Various EDP's

The probability of exceedance of the engineering demand parameters conditioned on the earthquake scenario that affected each bridge was computed using Eq. 1.

$$P(EDP > edp \mid Earthquake) = \int P(EDP > edp \mid D_H = d_h) \left| dP(D_H > d_h \mid Earthquake) \right| \quad (1)$$

Eq. 1 was integrated numerically based on the discrete data obtained from the probabilistic lateral spreading ground displacement analysis (Fig. 9) and the fragility functions (Fig. 10). Lateral spreading ground displacement was binned into 100 values in the range from 0 to 2m. At the center of each bin $P(EDP>edp|D_H=d_h)$ was computed from the fragility functions (Fig. 10), and $dP(D_H>d_h|Earthquake)$ was computed as the difference in cumulative probability at the right and left sides of the bins in the lateral spreading ground displacement curves (Fig. 9). The product of these terms was summed over all 100 bins, and the process was repeated for each value of EDP in the fragility functions, and for each method of lateral spreading displacement predictions (Fig. 11).

A very useful interpretation of the results in Fig. 11 is to investigate how much dispersion exists in the prediction of the EDP's for the various lateral spreading estimation methods. The method used to estimate lateral spreading ground displacement produced significant differences for the Showa Bridge, moderate differences for Landing Road Bridge, and small differences for Leuw Mei Bridge. The explanation for this trend is the degree to which the structures were sensitive to the free-field ground surface displacement. The pile foundations at Showa Bridge were the weakest and most flexible relative to the lateral spreading soil, and therefore tended to move with the spreading ground. Hence, this bridge was very sensitive to the estimate of free-field lateral spreading displacement, and the method of estimating free-field displacement is important. On the other hand, the Leuw Mei Bridge caisson foundations were very stiff and strong and essentially insensitive to lateral spreading, which renders the method used to estimate lateral spreading displacement less important. Since estimating lateral spreading deformation is such an uncertain calculation, designing structures that are insensitive to lateral spreading obviously improves reliability.

A related observation is that predictions were more accurate in cases that exhibited good performance than for cases that exhibited poor performance. All three ground displacement estimation methods correctly predicted good performance at Leuw Mei Bridge. A bit more variation was present in the predictions for Landing Road Bridge, where moderate damage occurred, and the most significant variations occurred for Showa Bridge, which collapsed. This observation may have little influence on design of new bridges, where good performance is always targeted, but may be quite important for retrofit evaluation of older structures, where marginal performance is sometimes predicted. This study shows that accurately predicting mediocre performance may be very difficult, and engineers should avoid relying on deterministic predictions in such cases because probability of mobilizing worse performance may be unacceptably high.

Conclusions

Static BNWF analyses of pile foundations and pier columns reasonably predicted the response of foundations at three different sites that suffered various levels of damage due to liquefaction and lateral spreading in past earthquakes. The analyses predicted the performance of each bridge quite well when the measured lateral spreading demands were imposed on the bridge. However, these demands are highly uncertain and different approaches for estimating lateral spreading displacement provided vastly different predictions. Utilizing multiple methods to estimate ground surface displacement is recommended to account for epistemic uncertainty. Life safety decisions should not depend on an estimate of ground displacement that utilizes a single method.

Foundations that are stiff and strong and do not deform excessively as laterally spreading soil flows past are less sensitive to lateral spreading ground displacements compared with foundations that move along with the soil. Therefore, designs that provide good performance are also more reliable, whereas significant risk may be inadvertently accepted for weak flexible foundations that move with laterally spreading soil. Designing foundations that are stiff and strong relative to the laterally spreading soil may not be feasible, particularly in cases where a thick, strong nonliquefied crust spreads atop underlying liquefiable layers. Ground improvement may be required to provide adequate reliability in such cases.

The probabilistic approach adopted in this study provides a rational basis for assessing how much risk is associated with a particular design, and provides a superior decision-making framework compared with deterministic methods. The calculations required to generate the lateral spreading displacement hazard curves are quite modest, yet the information gleaned from these calculations is very valuable. The calculations required to generate the fragility functions are more onerous, but easily approachable in analytical frameworks that can be controlled using scripting languages such as the TCL language that controls OpenSees. The calculations required to integrate the lateral spreading displacement hazard curve with the fragility functions are trivial. Hence, probabilistic calculations introduce a modest increase in effort compared with deterministic methods, but provide valuable information that may justify the effort in many cases.

Acknowledgements

Funding for this work was provided by the California Department of Transportation and the National Science Foundation through the Pacific Earthquake Engineering Research Center under project no. SA5407:1 (Caltrans) and SA5258 (NSF). Tom Shantz was the technical coordinator for the contracts. The contents of this paper do not necessarily represent a policy of either funding agency or endorsement by the state or federal government. The authors are grateful to Daniel Chu and P.S. Lin for gathering information for the Leuw Mei Bridge, and to Allison Faris for providing input on appropriate use of her lateral spreading model with uncertain ground motions in the forward predictions.

References

Abrahamson, N., Atkinson, G., Boore, D., Bozorgnia, Y., Campbell, K., Chiou, B., Idriss, I.M., Silva, W., and Youngs, R. (2008). "Comparisons of the NGA ground-motion relations." *Earthquake Spectra*, 24(1), 45-66.

Abrahamson, N. A., and Silva, W. J., (2008). "Summary of the Abrahamson & Silva NGA groundmotion relations", *Earthquake Spectra* **24**, 67–97.

API(1993). *Recommended Practice for Planning, Design, and Constructing Fixed Offshore Platforms*. API RP 2A - WSD, 20th ed., American Petroleum Institute.

Ashford, S.A., and Juirnarongrit, T. (2003). "Response of single piles and pipelines in liquefaction-induced lateral spreads using controlled blasting." *Earthquake Engineering and Engineering Vibration*, 1(2), 181-194.

Berrill, J. B., Christensen, S. A., Keenan, R. P., Okada, W., and Pettinga, J. R. (2001). “Case study of lateral spreading forces on a piled foundation.” *Geotechnique*, 51(6). 501-517.

Bhattacharya, S., Madabhushi, S. P. G., Bolton, M. D., Haigh, S. K., and Soga, K. (2003). *A Reconsideration of the Safety of Piled Bridge Foundations in Liquefiable Soils*, Technical Report CUED/D-SOILS/TR 328, University of Cambridge, UK, 1-31.

Bolton, M.D. (1986). "The strength and dilatancy of sands." *Geotechnique*, 36(1), 65-78.

Boore, D. M., and Atkinson, G. M., (2008). "Ground-motion prediction equations for the average horizontal component of PGA, PGV, and 5%-damped PSA at spectral periods between 0.01 s and 10.0 s.", *Earthquake Spectra* **24**, 99–138.

Boulanger, R.W., and Tokimatsu, K. (2006). "Seismic performance and simulation of pile foundations in liquefied and laterally spreading ground." ASCE GSP No. 145. 321p.

Boulanger, R. W., Chang, D., Brandenberg, S. J., Armstrong, R. J., and Kutter, B. L. (2007). "Seismic design of pile foundations for liquefaction effects." *Earthquake Geotechnical Engineering*, 4th International Conference on Earthquake Geotechnical Engineering – Invited Lectures, K. D. Pitilakis, ed., Springer, The Netherlands, 277-302.

Brandenberg, S. J. (2005). "Behavior of pile foundations in liquefied and laterally spreading ground." Ph.D. Thesis, University of California, Davis.

Brandenberg, S.J., and Kashighandi, P. (2011). "Influence of underlying weak soil on passive earth pressure in cohesionless deposits." J. Geotech. and Geoenviron. Eng., 137(3), 273-278.

Brandenberg, S. J., Boulanger, R. W., Kutter, B. L., and Chang, D. (2007). "Static pushover analyses of pile groups in liquefied and laterally spreading ground in centrifuge tests." *Journal of Geotechnical and Geoenvironmental Engineering*, 133(9), 1055-1066.

Brandenberg, S.J., Bellana, N., and Shantz, T. (2010). "Shear wave velocity as function of standard penetration test resistance and vertical effective stress at California bridge sites." Soil Dynamics and Earthquake Engineering, 30(10), 1026-1035.

Bray, J. D., and Travasarou, T. (2007). "Simplified procedure for estimating earthquake-induced deviatoric slope displacements." *Journal of Geotechnical and*

Geoenvironmental Engineering, 133(4), 381-392.

Campbell, K.W., and Bozorgnia, Y. (2008). "NGA ground motion model for the geometric mean horizontal component of PGA, PGV, PGD and 5% damped linear elastic response spectra for periods ranging from 0.01 to 10 s." *Earthquake Spectra* **24**, 139–171.

Cetin, K. O., Seed, R. B., Der Kiureghian, A., Tokimatsu, K., Harder, L. F. Jr., Kayen, R. E., and Moss, R. E. S. (2004). "SPT-based probabilistic and deterministic assessment of seismic soil liquefaction potential." *Journal of Geotechnical and Geoenvironmental Engineering*, 130(12), 1314-1340.

Chiou, B. S. J., and Youngs, R. R., (2008). "Chiou-Youngs NGA ground motion relations for the geometric mean horizontal component of peak and spectral ground motion parameters", *Earthquake Spectra* **24**, 173–215.

Chu, D. B., Brandenberg, S. J., and Lin, P. S. (2008). "Performance of bridges in liquefied ground during 1999 Chi-Chi earthquake." *Proceedings of the 14th World Conference on Earthquake Engineering*, in press.

Chu, D. B., Stewart, J. P., Youd, T. L., and Chu, B. L. (2006). "Liquefaction-induced lateral spreading in near-fault regions during the 1999 Chi-Chi, Taiwan earthquake." *Journal of Geotechnical and Geoenvironmental Engineering*, 132(12), 1549-1565.

Dobry, R., Taboada, V, and Liu., L. (1995). "Centrifuge modeling of liquefaction effects during earthquakes." *Proc. 1st Intl. Conf. On Earthquake Geotechnical Engineering*, K. Ishihara, ed., Tokyo, Japan, Vol. 3, pp. 1291-1324.

Dobry, R., Abdoun, T., O'Rourke, T. D., and Goh, S. H. (2003). "Single piles in lateral spreads: field bending moment evaluation." *J. Geotech. Geoenviron. Eng.*, 129(10), 879-889.

Faris, A. T., Seed, R. B., Kayen, R. E., and Wu, J. (2006). "A semi-empirical model for the estimation of maximum horizontal displacement due to liquefaction-induced lateral spreading." *8th National Conference on Earthquake Engineering*, EERI, San Francisco, CA

Field, E.H., T.H. Jordan, and C.A. Cornell (2003), OpenSHA: A Developing Community-Modeling Environment for Seismic Hazard Analysis, *Seismological Research Letters*, **74**, no. 4, p. 406-419.

Fukuoka, M. (1966). "Manage to civil engineering structures." *Soil and Foundation*, 6(2), 45-52.

González, L., Abdoun, T., and Dobry, R. (2009). "Effect of soil permeability on centrifuge modeling of pile response to lateral spreading." *J. Geotech. Geoenviron. Eng.* 135(1), 62-73.

Hamada, M., and O'Rourke, T. D. (1992). *Case Studies of Liquefaction and Lifeline Performance during Past Earthquakes: Volume 1 Japanese Case Studies*, Technical Report NCEER-92-0001, State University of New York at Buffalo, 3: 1-28.

Idriss, I. M., and Boulanger, R. W. (2008). "Soil liquefaction during earthquakes." Monograph MNO-12, Earthquake Engineering Research Institute, Oakland, CA, 261 pp.

Idriss, I. M., and Boulanger, R. W. (2006). “Semi-empirical procedures for evaluating liquefaction potential during earthquakes.” *Journal of Soil Dynamics and Earthquake Engineering*, 26, 115-130.

Idriss, I. M., 2008. An NGA empirical model for estimating the horizontal spectral values generated by shallow crustal earthquakes, *Earthquake Spectra* **24**, 217–242.

Jibson, R. W., and Jibson, M. W. _2003_. “Java programs for using Newmark’s method and simplified decoupled analysis to model slope performance during earthquakes.” *U.S. Geological Survey Open-File Rep. No. 03–005*, Washington, D.C.

Kerciku, A A, Bhattacharya, S, Lubkowski, Z A & Burd, H J. (2008). "Failure of Showa Bridge during 1964 Niigata earthquake: Lateral spreading or buckling instability?", 14th World Conference on Earthquake Engineering, Beijing.

Kulasingam, R., Malvick, E. J., Boulanger, R. W., and Kutter, B. L. (2004). “Strength loss and localization at silt interlayers in slopes of liquefied sand.” *J. Geotech. Geoenviron. Eng.*, 130(11): 1192–1202.

Ledezma, C., and Bray, J.D. (2010). "Probabilistic performance-base procedure to evaluate pile foundations at sites with liquefaction-induced lateral displacement." *J. Geotech. Geoenviron. Eng.* 136(3), 464-476.

Marcuson, W.F., and Hynes, M.E. (1990). "Stability of slopes and embankments during earthquakes." *Proc. ASCE/Pennsylvania Dept. of Transportation Geotechnical Seminar*, Hershey, Pennsylvania.

McKenna, F.T. (1997). "Object-oriented finite element programming: Frameworks for analysis, algorithms and parallel computing," PhD Thesis, Department of Civil Engineering, University of California, Berkeley.

Olson, S. M., and Johnson, C. I. (2008) “Analyzing liquefaction-induced lateral spreads using strength ratios.” *Journal of Geotechnical and Geoenvironmental Engineering*, 134(8): 1035-1049.

Olson, S. M., and Stark, T. D. (2002). “Liquefied strength ratio from liquefaction flow failure case histories.” *Can. Geotech. J.*, 39, 629–647.

Rollins, K. M., Gerber, T. M., Lane, J. D., and Ashford, S. A. (2005). “Lateral resistance of a full-scale pile group in liquefied sand.” *Journal of Geotechnical and Geoenvironmental Engineering*, 131(1): 115-125.

Terzaghi, K. (1955). "Evaluation of coefficients of subgrade reaction." *Geotechnique*, 5(4), 297-326.

Wilson, D. W., Boulanger, R. W., and Kutter, B. L. (2000). “Observed seismic lateral resistance of liquefying sand.” *Journal of Geotechnical and Geoenvironmental Engineering*, 126(10), 898-906.

Wilson, J. C. (2003). “Repair of new long-span bridges damaged by the 1995 Kobe earthquake.” Journal of Performance of Constructed Facilities, 17(4), 196-205.

Wu. J. (2002). "Liquefaction triggering and Post Liquefaction Deformations of Monterey 0/30 Sand under Uni-Directional Cyclic Simple Shear Loading. Ph.d. dissertation, University of California, Berkeley.

Yoshida, N., Tazoh, T., Wakamatsu, K., Yasuda, S., Towhata, I., Nakazawa, H., and Kiku, H. (2007). "Causes of Showa bridge collapse in the 1964 Niigata earthquake based on eyewitness testimony." *Soils and Foundations*, 47(6), 1075-1087.

Youd, T. L., Hansen, C. M., and Bartlett, S. F. (2002). “Revised MLR equations for prediction of lateral spread displacements.” *Journal of Geotechnical and Geoenvironmental Engineering*, 128(12), 1007-1017.

Youd, T. L., et al. (2001) “Liquefaction resistance of soils: summary report from the 1996 NCEER and 1998 NCEER⁄NSF workshops on evaluation of liquefaction resistance of soils.” *Journal of Geotechnical and Geoenvironmental Engineering*, 127(10), 817-833.

Zhang, G., Robertson, P. K., and Brachman, R. W. I. (2004). “Estimating liquefaction-induced lateral displacements using the standard penetration test or cone penetration test.” *Journal of Geotechnical and Geoenvironmental Engineering*, 130(8), 861-871.

Zhao, J.X., Zhang, J., Asano, A., Ohno, Y., Oouchi, T., Takahashi, T., Ogawa, H., Irikura, K., Thio, H.K., Somerville, P.G., Fukushima, Y., and Fukushima, Y. (2006). "Attenuation relations of strong ground motion in Japan using site classification based on predominant period." *Bulletin of the Seismological Society of America*, 96(3), 898-913.

Table 1. Case history descriptions.

Site	Earthquake	M_w	R_{jb} (km)	Style of Faulting	Nearest Measured Peak Horizontal Ground Acceleration	Measured Lateral Spreading Ground Displacement	Structural Configuration of Bridge	Liquefaction-Induced Damage
Showa Bridge	1964 Niigata	7.5	40	Reverse	0.16g in Kawagishi Cho, approximately 40km from epicenter and 1.2 km from Showa Bridge	Up to 4m at left bank, less than 1m at right bank	Simply-supported steel I-girders on bent caps supported by nine 0.62m diameter steel pipes.	Collapse of five spans
Landing Road Bridge	1987 Edgecumbe	6.3	8	Normal	0.33g at Matahina Dam, at R=8km from nearest surface rupture, 22km southwest of site	2m max., decreasing with distance upslope	Continuous reinforced concrete I-girders on groups of 0.42m square reinforced concrete piles	Cracking of piers and piles and residual rotations of 1° of piers
Leuw Mei Bridge	1999 Chi Chi	7.6	0.6	Thrust	0.42g in fault parallel direction at TCU076 station at R=1.1km from rupture, and 500m from Leuw Mei Bridge	0.25m at a distance 100m north of bridge. Spreading observed on both sides of river upstream and downstream of bridge, but only measured 100m north.	Six reinforced concrete box girder spans and one steel cable-stay span simply supported on 2m diameter pier columns on caisson foundations.	No liquefaction-induced damage, though the bearings were damaged due to strong shaking

Table 2. Input parameters for p-y elements.

	Showa Bridge P_4		Showa Bridge P_9		Landing Road Bridge			Leuw Mei Bridge		
	Loose Sand	Dense Sand	Loose Sand	Dense Sand	Silty Crust	Loose Sand	Dense Sand	Loose Sand	Dense Sand	Stiff Base Layer
Depth Range	0-10m	10-16m	0-5m	5-16m	0-1.2m	1.2-6.2m	6.2-10.5m	0-5m	5-14m	14-17m
c'	0	0	0	0	10 kPa	0	0	0	0	0
ϕ'	35°	40°	35°	40°	25°	37°	45°	40°	43°	47°
γ	19 kN/m^3	20 kN/m^3	19 kN/m^3	20 kN/m^3	12.5 kN/m^3	19 kN/m^3	20 kN/m^3	20 kN/m^3	20 kN/m^3	20 kN/m^3
Modulus of subgrade reaction K_{ref} [a]	38000 kN/m^3	76000 kN/m^3	38000 kN/m^3	76000 kN/m^3	N/A	40000 kN/m^3	90000 kN/m^3	76000 kN/m^3	90000 kN/m^3	160000 kN/m^3
p-multiplier m_p	0.1	0.9	0.1	0.9	1.0	0.1	1.0	0.1	1.0	1.0
Passive Force Acting on Pile Cap [b]	N/A	N/A	N/A	N/A	586 kN	N/A	N/A	N/A	N/A	N/A
y_{50} for p-y Elements on Pile Cap [c]	N/A	N/A	N/A	N/A	0.1m	N/A	N/A	N/A	N/A	N/A

(a) $K = K_{ref}\left(\frac{\sigma_v'}{0.5P_a}\right)^{0.5}$

(b) Passive force computed using Rankine earth pressure theory due to low friction along base of deposit (e.g., Brandenberg and Kashighandi 2011).

(c) y_{50} for the p-y elements on the pile cap was based on Brandenberg et al. (2007).

Table 3. Ground motion prediction for each earthquake.

	Nearest Measured PGA (g)	V_{s30} (m/s)[1]	Boore and Atkinson (2008)		Chiou and Youngs (2008)		Abrahamson and Silva (2008)		Campbell and Bozorgnia (2008)		Zhao et al. (2006)	
			PGA (g)	σ_{lnPGA}	PGA (g)	σ_{lnPGA}	PGA (g)	σ_{lnPGA}	PGA (g)	σ_{lnPGA}	PGA (g)	σ_{lnPGA}
1964 Niigata	0.16	226	NA	NA	NA	NA	NA	NA	NA	NA	0.27	0.72
1987 Edgecumbe	0.29	230	0.19	0.57	0.22	0.51	0.24	0.51	0.24	0.46	NA	NA
1999 Chi Chi	0.42	250	0.47	0.56	0.62	0.45	0.49	0.42	0.41	0.44	NA	NA

[1] Geophysical measurements of V_{s30} were not available, so they were computed based on correlation with blow count.

Table 4. Lateral spreading prediction using Youd et al. (2002) method.

Bridge	Boring	Mw	R (km)	T_{15} (m)	F_{15} (%)	$D50_{15}$ (mm)	S (%)	Predicted D_H (m)[a]	Measured Max. D_H (m)	Error
Showa	B1	7.5	30	12	10	0.31	1	1.63	4	-59%
	B2	7.5	30	10	10	0.31	1	1.48	N.A.	N.A.
	B3	7.5	30	7	10	0.31	1	1.22	N.A.	N.A.
	B4	7.5	30	3	10	0.31	1	0.77	0.5	54%
Leuw Mei	NCS1	7.6	0.6	1.7	22.3	0.12	3.8	12.91	0.25	5064%
	NCS2	7.6	0.6	1.7	22.3	0.12	3.8	12.91	0.25	5064%
Landing Road	BH12	6.3	8	3.5	12	0.35	3	0.24	2	-88%
	BH11	6.3	8	4.5	12	0.35	3	0.27	2	-86%
	R1	6.3	8	4.8	12	0.35	3	0.28	2	-86%

[a] If D_H>6, the result may be inaccurate and should be interpreted that large ground displacements might occur (Youd et al. 2002).

Table 5. Example calculation of ground displacement using Faris et al. (2006) method with median values of input parameters.

M_w	7.6	Moment magnitude
$\mu_{PGA\ (g)}$	0.50	Mean of PGA
σ_{PGA}	0.47	Standard deviation of natural logs of PGA
PGA (g)	0.50	Realization of PGA computed as $\exp[\mathrm{rnorm}(\ln(\mu_{PGA}),\sigma_{PGA})]^{a,b}$
V_{s12} (m/s)	200	Average shear wave velocity in upper 12m
z_{gwt} (m)	1.0	Depth to ground water table

Depth (m)	Δz (m)	$(N_1)_{60cs}$	Soil Type	Potentially Susceptible to Liquefaction?	σ_v (kPa)	σ_v' (kPa)	r_d [c]	CSR [d]	Strain Potential Index, SPI (%) [e]	Δz (m)	SPI*Δz (m)
1.4	0.4	17	Silty Sand	yes	27	24	0.99	0.37	28	0.4	0.1
2.4	1.0	12	Silty Sand	yes	46	33	0.99	0.45	56	1.0	0.6
3.4	1.0	15	Silty Sand	yes	66	43	0.98	0.49	42	1.0	0.4
4.4	1.0	10	Gravel with Sand	no	86	53	0.96	0.51	0	1.0	0.0
5.4	1.0	21	Gravel with Sand	no	106	63	0.95	0.52	0	1.0	0.0
6.4	1.0	28	Gravel with Sand	no	127	74	0.93	0.52	0	1.0	0.0
7.4	1.0	21	Gravel with Sand	no	149	86	0.90	0.51	0	1.0	0.0
8.9	1.5	30	Gravel with Sand	no	183	105	0.86	0.49	0	1.5	0.0
10.4	1.5	25	Silt	yes	214	120	0.81	0.47	15	1.5	0.2
11.4	1.0	29	Silt	yes	235	131	0.77	0.45	9	1.0	0.1
12.4	1.0	33	Silt	yes	256	143	0.74	0.43	5	1.0	0.1
13.4	1.0	30	Silt	yes	278	154	0.71	0.42	7	1.0	0.1
14.4	1.0	58	Silty Sand	yes	298	165	0.69	0.40	0	1.0	0.0
15.4	1.0	50	Silty Sand	yes	319	176	0.67	0.39	0	1.0	0.0
16.4	1.0	58	Silty Sand	yes	341	187	0.65	0.39	0	1.0	0.0
17.4	1.0	53	Silty Sand	yes	363	199	0.64	0.38	0	1.0	0.0

DPI_{avg} (m) = ΣSPI*Δz 1.5

D_{Havg}(m) = $\exp[\mathrm{rnorm}(0.7196*\ln(DPI_{avg}),0.4475)]$ 1.3

a PGA and D_{Havg} set equal to mean value for this example.

b rnorm(μ,σ) returns a normally distributed random number

c Mean values from Cetin et al. (2004)

d $CSR = 0.65 \dfrac{PGA}{g} \dfrac{\sigma_v}{\sigma_v'} r_d$

e Wu (2002) with extrapolation beyond SPI=50% by Faris (2004)

Table 6. Summary of ground displacements using Faris et al. (2006) method.

Bridge	Boring	Predicted D_H (m)	Measured D_H (m)	Error
Showa	B1	5.40	4	35%
	B2	5.00	N.A.	N.A.
	B3	3.10	N.A.	N.A.
	B4	0.50	0.5	0%
Leuw Mei	NCS1	0.70	0.25	180%
	NCS2	1.30	0.25	420%
Landing Road	BH12	1.20	2	-40%
	BH11	0.88	2	-56%
	R1	1.47	2	-27%

Table 7. Ground displacement predictions using Newmark sliding block approach using median input parameters.

Bridge	Mw	$(N_1)_{60}$ [a]	σ_v (kPa)	σ_v' (kPa)	s_r/σ_v'	s_r (kPa)	S (%)	k_y [b]	a_{max} [c]	Predicted D_H (m)	Measured D_H (m)	Error
Showa - P4	7.5	8	125	70	0.09	6	1	0.04	0.15	0.11	4	-97%
Showa - P9	7.5	12	145	64	0.12	8	1	0.04	0.15	0.10	0.5	-81%
Leuw Mei	7.6	13	55	38	0.13	5	3.8	0.05	0.50	0.78	0.25	212%
Landing Road	6.3	10	36	25	0.11	3	3.0	0.04	0.22	0.21	2	-89%

[a] Taken as average within zone with factor of safety against liquefaction less than 1.

[b] Based on infinite slope analysis.

[c] Mean of four ground motion prediction equations

Table 8. Distributions of input parameters for fragility function analysis.

Parameter	μ	σ	range	distribution
$(m_p)_{LooseSand}$	0.1	0.015	> 0	Truncated Normal
$(m_p)_{DenseSand}$	0.4	0.02	> 0	Truncated Normal
$\Delta_{slip}/\Delta_{crust}$ [a]	0.5	0.5	0-1	Uniform
F_I [b] Showa	48kN	83kN	> 0	Log-Normal
S_d [c] Landing Road	0.018m	0.030m	> 0	Log-Normal
F_{crust} [d] Landing Road	850kN	250kN	> 0	Truncated Normal
F_I [b] Leuw Mei	809kN	1332kN	$0 < F_I < 1275$kN [e]	Truncated Log-Normal

[a] $\Delta_{slip}/\Delta_{crust}$ is the ratio of the slip displacement at the loose sand-crust interface to the ground surface displacement caused by void redistribution (applied to Landing Road Bridge only).

[b] F_I is the inertia force acting on the top of the foundation.

[c] S_d is the displacement acting on the top of the foundation.

[d] F_{crust} is the total lateral force capacity of the p-y elements in the crust layer.

[e] The inertia demand cannot exceed the capacity of the reinforced concrete bearings, which is 1275kN.

Figure 1

Click here to download high resolution image

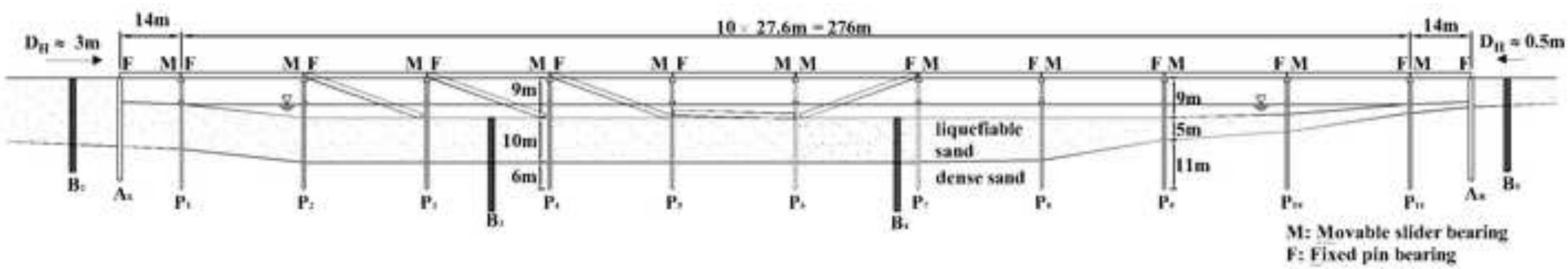

Figure 2
Click here to download high resolution image

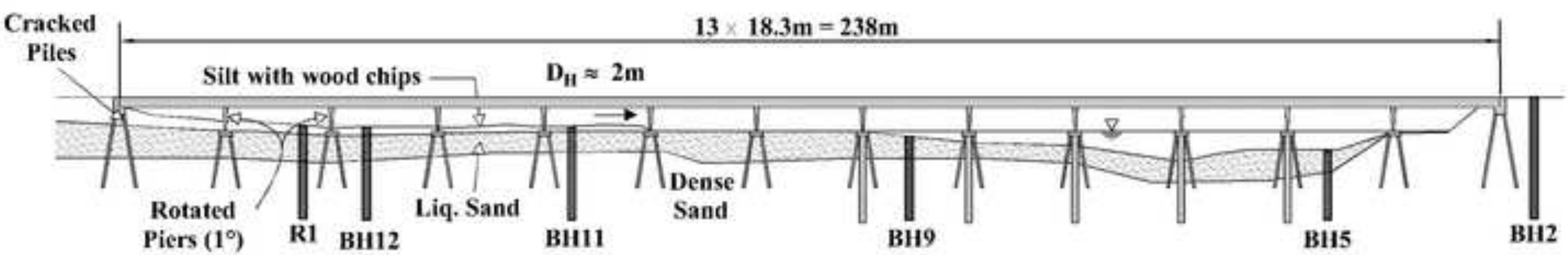

Figure 3
Click here to download high resolution image

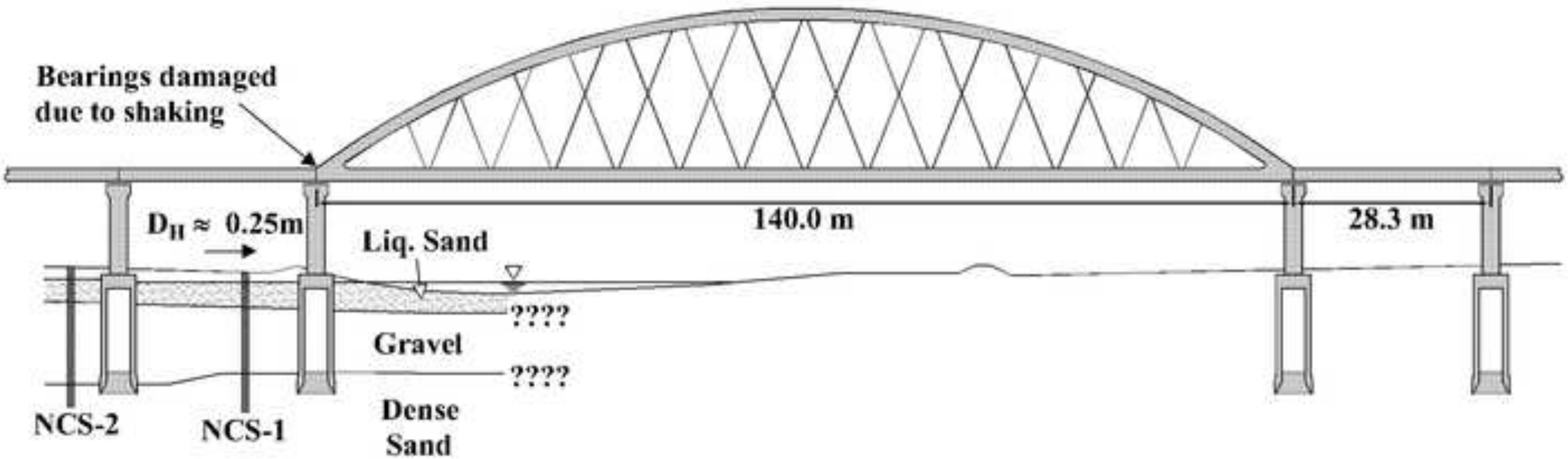

Figure 4

Click here to download high resolution image

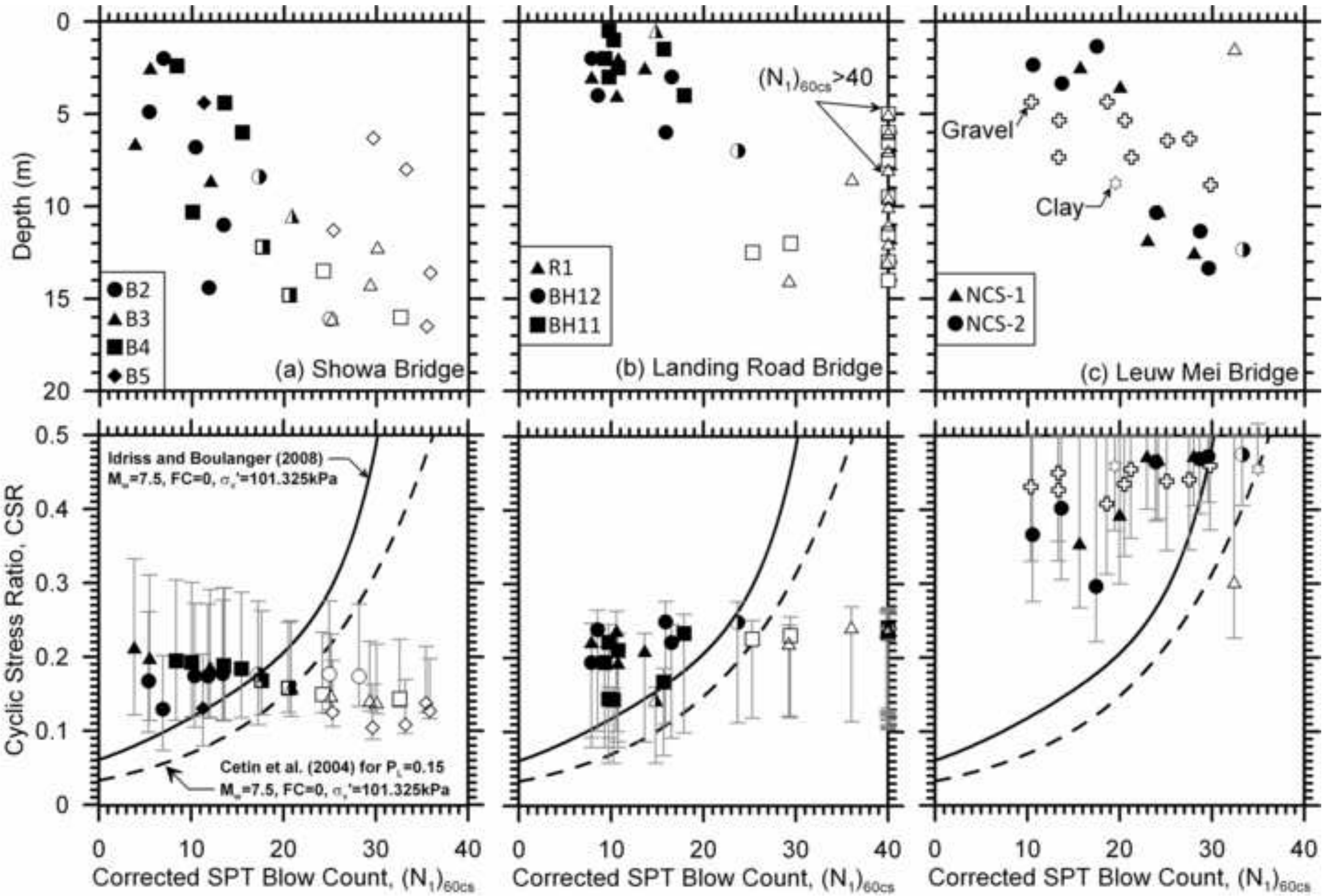

Figure 5
Click here to download high resolution image

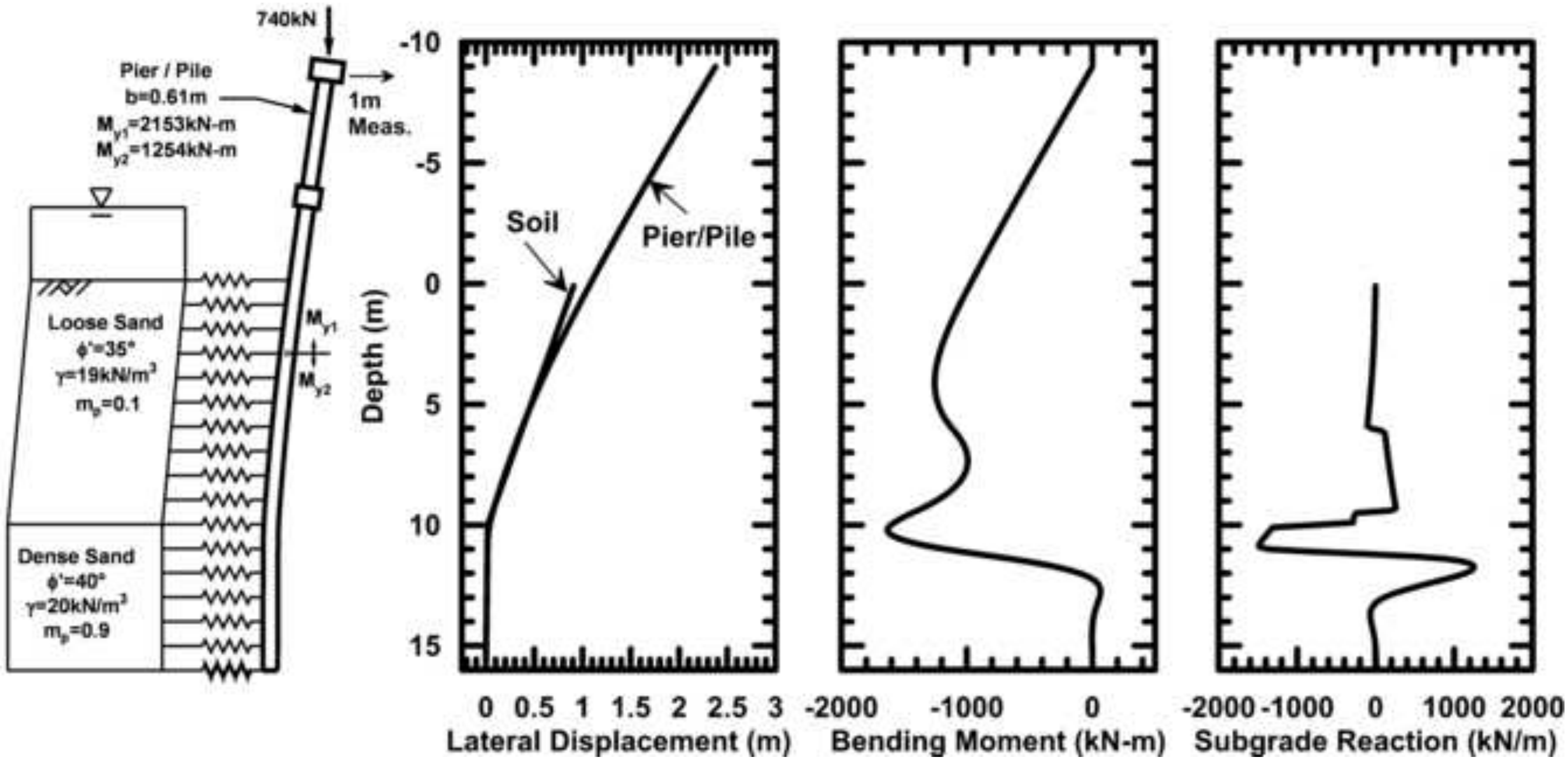

Figure 6
Click here to download high resolution image

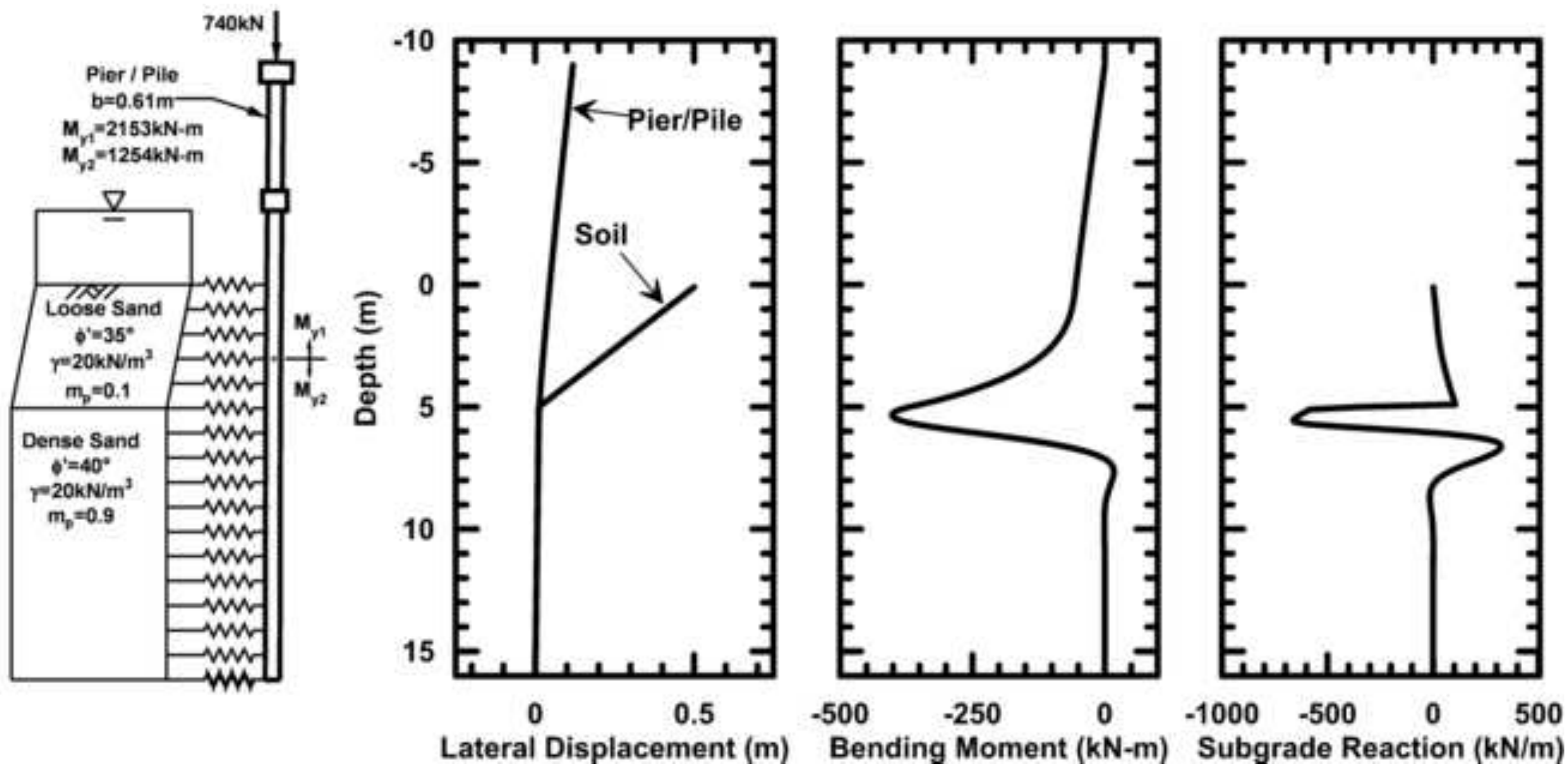

Figure 7
Click here to download high resolution image

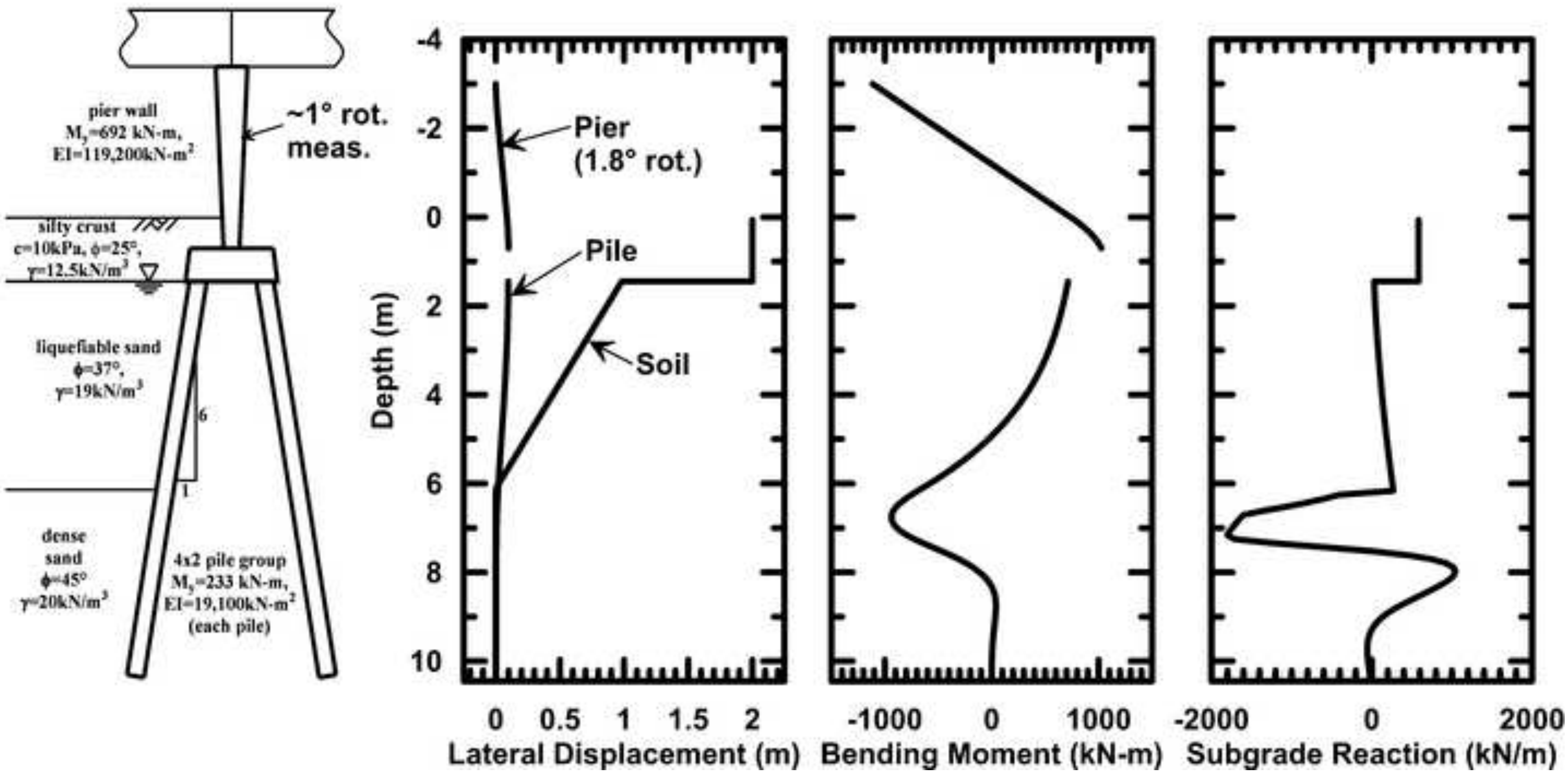

Figure 8

Click here to download high resolution image

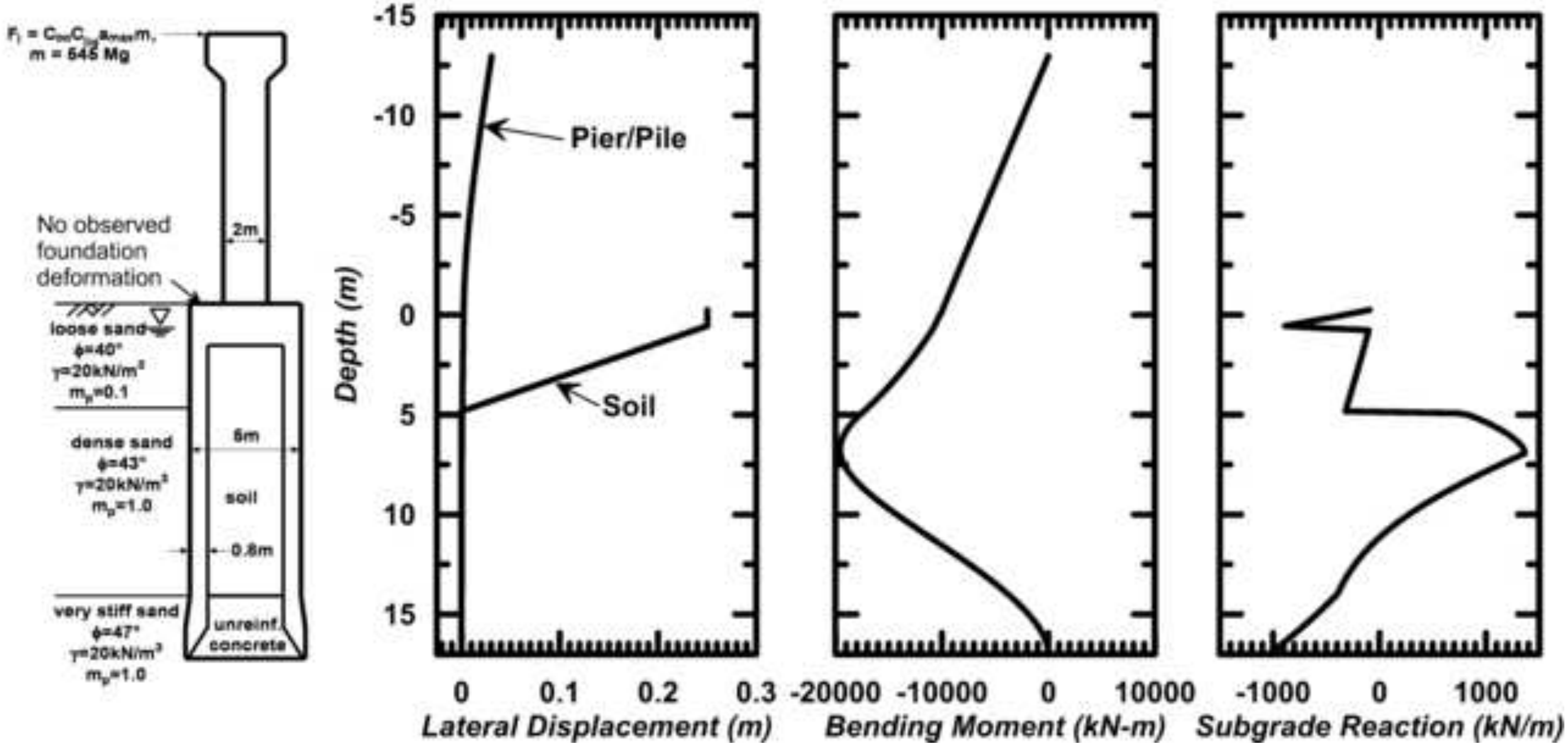

Figure 9

Click here to download high resolution image

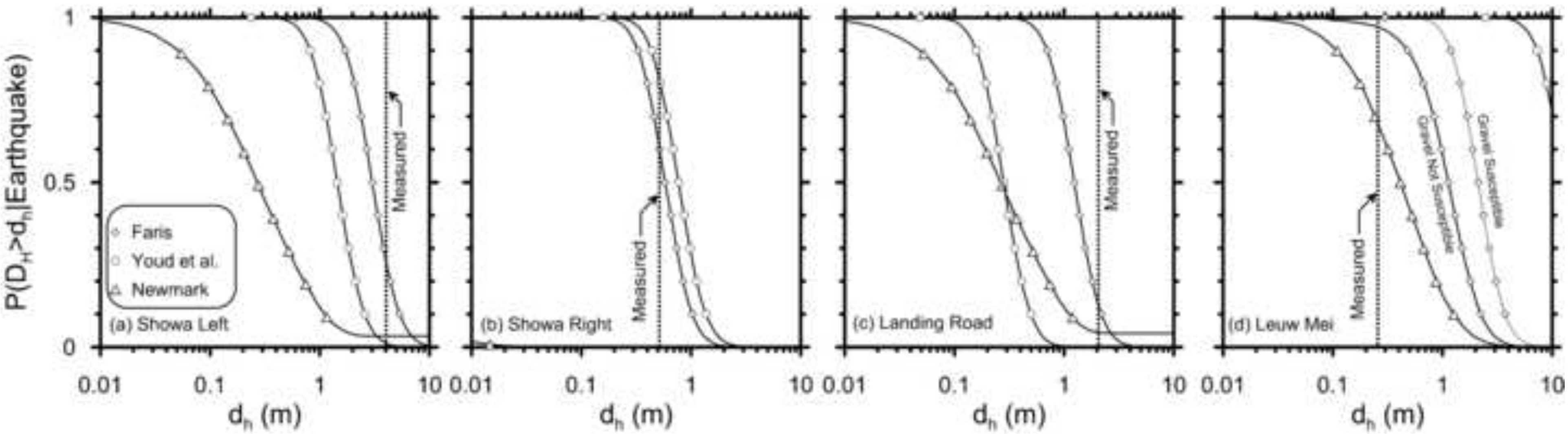

Figure 10
Click here to download high resolution image

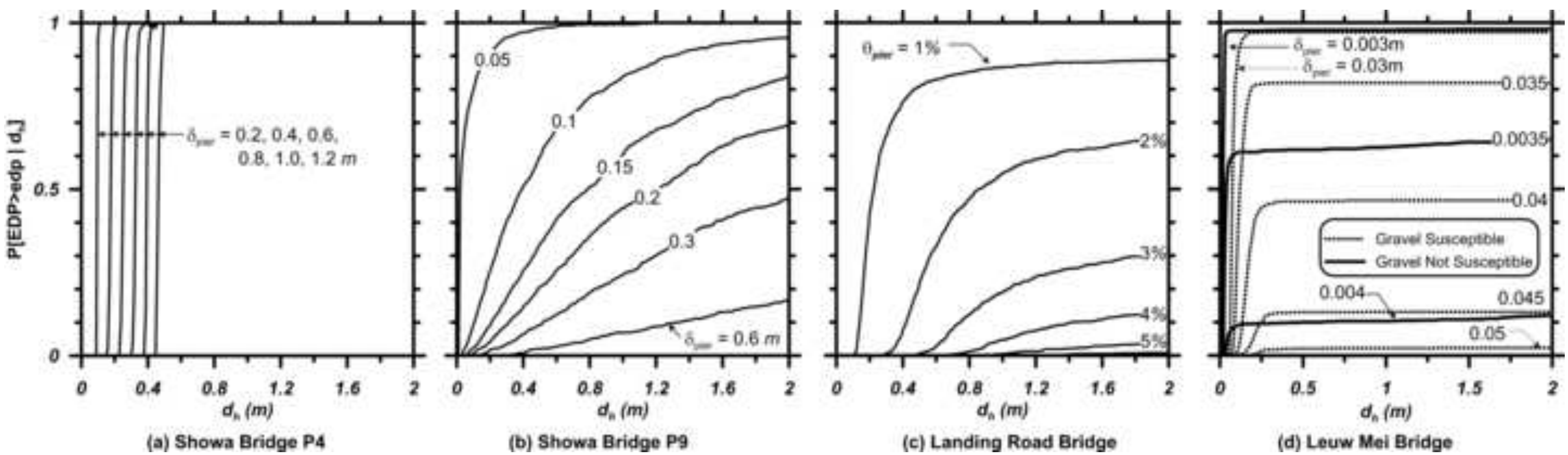

Figure 11
Click here to download high resolution image

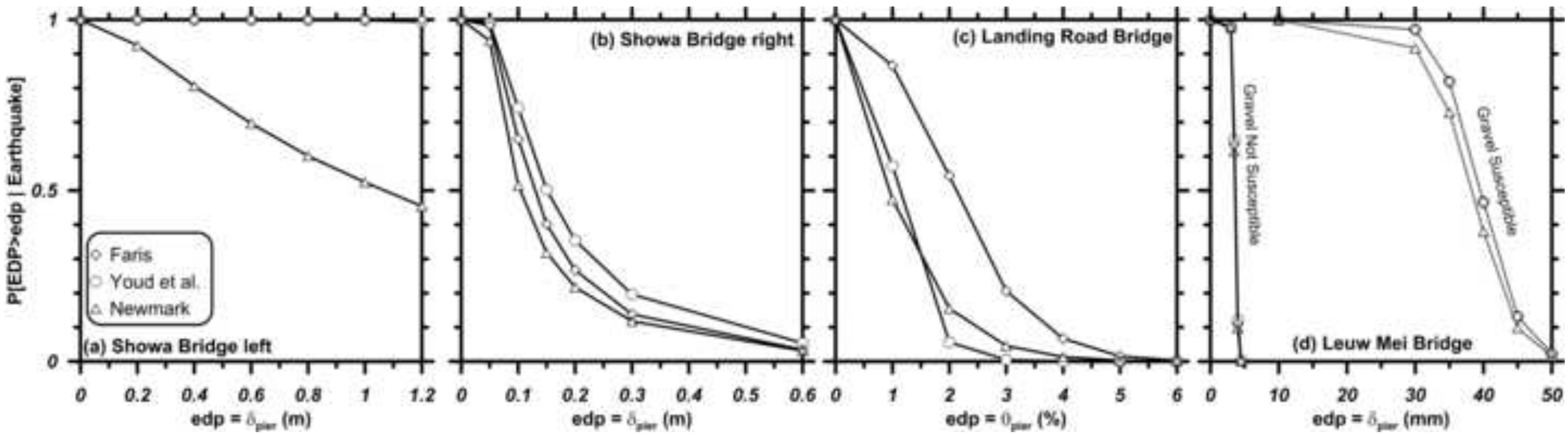

Figure 1. Schematic of collapse of Showa Bridge following the 1964 Niigata earthquake (after Hamada 1992).

Figure 2. Schematic of Landing Road Bridge following the 1987 Edgecumbe earthquake (after Berrill et al. 2001).

Figure 3. Schematic of Leuw Mei Bridge following 1999 Chi-Chi earthquake (after Chu et al. 2008).

Figure 4. Corrected SPT blow count $(N_1)_{60cs}$ versus depth and versus cyclic stress ratio for (a) Showa Bridge, (b) Landing Road Bridge, and (c) Leuw Mei Bridge. Symbols in the CSR plots were computed using nearest measured peak horizontal acceleration, and error bars were computed using the NGA GMPE's corresponding to $\pm 1\sigma$ predictions.

Figure 5. Analysis of pier P_4 for Showa Bridge. Measured ground surface displacements as high as 3m could not be imposed on the model due to numerical instability resulting from collapse mechanism forming at approximately 0.9m of soil surface displacement.

Figure 6. Analysis of pier P_9 for Showa Bridge using measured ground surface displacement of 0.5m to develop free-field soil displacement profile.

Figure 7. Analysis of Landing Road Bridge foundation and pier using measured ground displacement of 2m to develop free-field soil displacement profile.

Figure 8. Analysis of Leuw-Mei Bridge caisson and pier column using measured ground displacement of 0.25m to guide free-field soil displacement profile.

Figure 9. Probability of exceedance of lateral spreading displacement conditioned on the observed earthquake.

Figure 10. Fragility functions expressing key engineering demand parameters as functions of free-field lateral spreading displacement.

Figure 11. Probability of exceedance of the most relevant engineering demand parameter conditioned on the observed earthquake.